Comparison of Bulk- and Surface- Micromachined Pressure Sensors

William P. Eaton*, James H. Smith*, David J. Monk†, Gary O'Brien†, and Todd F. Miller†
* Sandia National Laboratories, Mail Stop 1081, Albuquerque, NM 87185
†Motorola, 5005 E. McDowell Rd, MS D138, Phoenix, AZ 85008

ABSTRACT

Two piezoresistive micromachined pressure sensors were compared: a commercially available bulk-micromachined (BM) pressure sensor and an experimental surface-micromachined (SM) pressure sensor. While the SM parts had significantly smaller die sizes, they were outperformed in most areas by the BM parts. This was due primarily to the smaller piezoresistive gauge factor in the polysilicon piezoresistors in the SM parts compared to the single crystal strain gauge used in the BM parts.

1. INTRODUCTION

Surface-micromachining (SM) has become an increasingly popular technology in recent years, with potential advantages over bulk micromachining (BM) such as smaller device size and CMOS compatibility. In this paper, we evaluate surface-micromachining technology by a *vis a vis* comparison of two piezoresistive pressure sensors: (1) an experimental SM sensor developed at Sandia National Laboratories and (2) a commercially available MPX200 BM sensor developed at Motorola.

The discovery of piezoresistivity in silicon and germanium in 1954 [1] enabled the production of semiconductor-based sensors. Silicon strain-gauge, metal-diaphragm sensors were first introduced commercially in 1958 [2]. Micromachined pressure sensors were available in 1963 [3] and advances in fabrication technology have led to the bulk-micromachined sensors available today. By contrast, surface micromachined pressure sensors are relative newcomers, first reported in 1985 [4] and 1986 [5] with other reports following thereafter [6,7,8,9,10].

There has been much debate over which technology is better, SM or BM. Key technology differences are illustrated by the fabrication sequences in the FABRICATION section of this paper. A more detailed treatment of fabrication technologies is given in [11]. Some of the relative merits of both technologies are summarized in Table 1. Material properties of single crystal silicon used in BM are superior to deposited films used in SM. Single crystal silicon has few defects and mechanical properties such as Young's modulus and Poisson's ratio are expected to be very repeatable, in contrast to polysilicon films, whose properties will vary strongly with processing conditions. While single crystal silicon wafers are nearly stress free, polysilicon films can have a range of compressive or tensile stresses. Also, the piezoresistive gauge factor of single crystal silicon is significantly greater than deposited polysilicon. The relative costs of producing parts in both technologies is a function of the volume. Capital costs for BM equipment are generally lower than SM costs and hence BM will have lower costs for small volumes. For high volumes, however, smaller die size of SM parts will tend to make them more economical.

Dimensional control of micromechanical structures is strongly related to performance. Lot to lot, wafer to wafer, and wafer center to wafer edge variabilities are all undesirable. BM geometries are constrained largely by the characteristic 54.7° angle of anisotropic etching [11,12]. Wafer thickness variations can lead to uncertainties in etched diaphragm thicknesses. SM dimensions are generally smaller with lateral variations due to photolithography and etching and vertical variations due to deposition thicknesses.

SM devices are often touted as being more compatible with monolithic CMOS integration than BM parts: that is, the cofabrication of MEMS devices and CMOS on a single substrate. Three reasons are responsible for this phenomenon: (1) a reluctance to allow parts potentially contaminated with potassium (from KOH etching); (2) reluctance to allow processing of potentially fragile bulk micromachined substrates; and (3) backside fabrication is not common in CMOS foundries, and is required for BM.

While the capital cost of SM equipment is greater than BM, SM is considered to be more compatible with on-chip CMOS processing. Also, dimensional control of SM parts is generally better, and SM parts are smaller than their BM counterparts.

Packaging of nearly any micromachined device presents challenges when compared to microelectronics.

Table 1. Comparison of Surface- and Bulk-micromachining technologies

Parameter		SM	BM
Mechanical properties		Good	Superior
Cost:	Low volume	Fair	Good
	High volume	Good	Fair
Dimensional control		Better	Good
CMOS integration		Good	Fair
Packaging		Fair	Fair
Size		Smaller	Small

One of the significant differences in BM and SM parts presented in this work is that BM pressure sensors appear to be more sensitive to packaging induced stresses.

Surface micromachined parts will generally be smaller than bulk micromachined parts for similar performance. This is mainly because the subtractive techniques used for BM are less controllable than the additive techniques used for SM.

Consider the following diaphragm deflection example. Since the output signal of a piezoresistive pressure sensor is directly proportional to diaphragm deflection, diaphragm deflection can be used as a tool for comparison. Consider the deflection, y, of a circular diaphragm under an applied pressure [13]

$$y = \frac{3}{16} \frac{Pa^4 (1 - v^2)}{Eh^3},$$

where a, v, E, and h are diaphragm radius, Poisson's ratio, Young's modulus, and thickness, respectively. Generally BM diaphragms must be a little thicker, since final thickness is difficult to control due to wafer thickness variations. Thickness of SM diaphragms is controlled by the thickness of LPCVD depositions, which are generally quite uniform. If we compare a 1 µm thick SM diaphragm to a 10 µm thick BM diaphragm (with identical materials properties), to yield the same amount of deflection under the same amount of pressure we must have

$$\frac{a_{BM}}{a_{SM}} = \sqrt[4]{\frac{h_{BM}}{h_{SM}}} = \sqrt[4]{\frac{10 \, \mu m}{1 \mu m}} \approx 5.6,$$

so that the SM diaphragm lateral dimensions are 5.6 times smaller than the BM dimensions.

2. THEORY OF OPERATION

The SM and BM sensors are shown schematically in Figure 1. Both sensors are based on piezoresistive strain gauges mounted on deformable diaphragms. Changes in ambient pressure cause diaphragm deflections and strains which give rise to resistance changes in the piezoresistors. For small deflections, the resistance change varies linearly with applied pressure.

The BM sensor (Figure 1, left) has a square single crystal diaphragm with a 1448 µm length and 26.5 µm thickness. A four terminal X-ducer™ [14] shear strain gauge is used to read pressure.

The SM sensor (Figure 1, right) has a circular poly-silicon diaphragm that is ≈ 2 µm thick. In theory, circular diaphragms will have an advantage over square or rectangular diaphragms due to the absence of stress concentrations at the corners. However, as shown in the cross section of Figure 1(right), the substrate provides a built-in overpressure stop. It has been demonstrated that overpressure resistance to fracture is excellent for even square and rectangular SM diaphragms [15]. An em-

Table 2 . Fabrication complications due to nonplanarity.

Fabrication Step	Associated topography problem
photolithography	poor step coverage, dep of focus
dry etching	stringer generation
metallization	step coverage
Ion implantation	dopant uniformity

bedded reference pressure cavity is underneath the diaphragm. A fully active Wheatstone bridge configuration is used to sense pressure, with two radial and two circumferential resistors. For this design, two diaphragms are required to make one Wheatstone bridge. The off-diaphragm ballast resistor is used to balance the pressure-free radial and circumferential resistor values. A reference design for a single diaphragm, ballast-less Wheatstone bridge sensor is shown in Figure 2.

3. FABRICATION

3.1 MPX200

The Motorola MPX200 fab sequence is shown in Figure 3. First, the silicon substrate is selectively ion implanted to form the X-ducer transducer (Figure 3a). Then, metal contacts are deposited and patterned, and the surface is passivated with a silicon nitride film (Figure 3b). The substrate is then bulk-micromachined to form the diaphragm (Figure 3c) . Finally, the sensor wafer is bonded to a handle wafer to form a reference pressure cavity (Figure 3d), if the device is to measure absolute pressure. A photograph of a packaged MPX200 is shown in Figure 4.

3.2 SNL

Both planar and non-planar sensors have been fabricated at Sandia National Laboratories. These are shown in Figure 5. Planar sensors are generally more manufacturable than non-planar sensors. The topography of the non-planar sensors complicates a number of fabrication steps, including photolithography, dry etching, ion implantation, and metallization. These problems are summarized in Table 2.

The planar fabrication sequence is depicted in Figure 6. First, deep and shallow trenches are formed by plasma etching and then are lined with silicon nitride (Figure 6a). The deep trench later becomes the reference pressure cavity, and the shallow trench serves as a release etch port. The trenches are then filled with undoped SiO_2 (Figure 6b) and the substrates are polished flat by chemical mechanical polishing (Figure 6c). Chemical mechanical polishing offers many advantages to the would-be surface micromachinist by reducing topographical constraints [7]. After planarization, the dia-

phragm material (polysilicon) is deposited and patterned for release etch (Figure 6d). The release etch is then performed by a wet etch in concentrated 1:1 HF:HCl (49% and 36% respectively) solution. The etch solution is displaced by deionized water overnight and the wafers are dried by setting them on the bench top. The diaphragm stiffness appears to keep the diaphragms from sticking to the trench below. The diaphragm is sealed by an LPCVD nitride deposition, which plugs the release etch ports and forms a reference cavity under partial vacuum (Figure 6f). A picture of a sealed etch hole is shown in Figure 7. Finally, a thin, 0.1 µm layer of polysilicon is deposited, implanted for maximum piezoresistive gauge factor [16], and patterned. Then aluminum is deposited and patterned (Figure 6g).

3.3 Assembly

Packaging of all parts occurred at the Motorola Sensor Product Division's prototype assembly lab. Assembly included wafer dicing, die attach, wirebond, leak testing, and porting with Motorola standard pressure sensor packages. Both top and dual piston fit packages were used (Figure 8). An elastomeric silicone die attach material (GE 6445) was used. It was dispensed in a solid strip under the rectangular die. Wirebonding was performed with 1 mil Au wire. No silicone gel encapsulation was used in this study.

4. EXPERIMENTAL RESULTS

Parts were tested using Motorola's Pressure Sensor Electrical Characterization (PSEC) system in the Sensor Engineering Support Lab. PSEC exposes parts to pressure and temperature conditions in a controlled environment to extract output characteristics of the pressure sensors. Standard data sheet parameters were then calculated. These parameters included: offset, sensitivity, linearity error, span, temperature coefficient of span (TCS), temperature coefficient of offset (TCO) and temperature hysteresis. In addition to these parameters, the pressure sensors were characterized for drift and ratio metricity error. Noise data was taken in a typical circuit, which consists of Motorola low noise amplifiers and a filtered battery power source. Peak and RMS voltages were recorded on a LeCroy 9314AL oscilloscope.

SM sensors with diaphragm diameters of 100, 150, and 200 µm were examined. Variations in sensitivity and nonlinearity as a function of diaphragm diameter are plotted in Figure 9 and Figure 10. The linear variation of sensitivity with diaphragm diameter is surprising, since small deflection theory predicts a square variation [13]. The discrepancy is explained by the presence of built-in thin film stress in both the polysilicon and overcoat of silicon nitride. This phenomenon is further exaggerated if silicon nitride diaphragms are used, where the sensitivity of the pressure sensors is independent of diaphragm diameter over a range of 50 µm to 250 µm[17,18].

The nonlinearity (or linear error) has larger uncertainty in the SM sensors for smaller diaphragms (Figure 10). This is due in part to the fact that smaller diaphragm sensors have a smaller span and hence variations in error become magnified. Additionally, smaller diaphragm sensors have been observed to be more noisy than larger diaphragms, which may account for some of the uncertainty.

Temperature Coefficient of Sensitivity and Offset (TCS and TCO) are graphed in Figure 11 and Figure 12 and don't appear to be a strong function of diaphragm size.

The 200 µm diameter SM sensor had the highest signal to noise ratio of the SM sensors and was chosen to compare to the MPX200. A 'data sheet' comparison of the two devices is shown in Table 3.

In many applications the analog signal from the pressure sensor will be converted to a digital signal that can be read by the end user. For these applications analog to digital (A/D) resolution is critical. A/D resolution shown in Table 4.

5. DISCUSSION AND CONCLUSIONS

Surface micromachining appears to have many advantages over bulk micromachining. In this paper we have attempted to compare SM and BM devices. In terms of raw device performance, the BM sensors were better for all measured parameters except TCS and TCO. The higher BM TCS and TCO are likely due to non-optimal stress isolation of the BM die from its package.

The principal reason for poorer SM device performance is the lower piezoresistive gauge factor of poly- vs. single crystalline silicon. Increased sensitivity could be achieved by using a capacitive sensor with integrated CMOS. While integration of pressure sensors with CMOS appears to be more practical with SM, more work is required to substantiate this statement.

Despite the lower performance of the SM sensor compared to the BM sensor, significantly smaller diaphragms were made, which translates to smaller overall die size. The differences in fabrication cost, yield, and packaging, and test costs between the two technologies is difficult to quantify, making overall device costs difficult to compare.

REFERENCES

[1] C. S. Smith, "Piezoresistance effect in germanium and silicon" Physical Review, **94**(1), pp. 42-49 (1954).

[2] J. Bryzek, K. Petersen, J. R. Mallon, L. Christel, and F. Pourahmadi, *Silicon Sensors and Microstructures*, Lucas Novasensor (1990).

[3] J. C. Sanchez, "Semiconductor strain-gauge pressure sensors", *Instruments and Control Systems*, pp. 117-120 (November 1963).

[4] H. Guckel, D. W. Burns, H. H. Busta, and J. F. Detry, "Laser-recrystallized piezoresistive microdiaphragm pressure sensor", in *Technical Digest, 1985 International Conference on Solid State Sensors and Actuators, Transducers '85*, pp. 182-185 (1985).

[5] S. Sugiyama, T. Suzuki, K. Kawahata, K. Shimaoka, M. Takigawa, and I. Igarashi, "Microdiaphragm pressure sensor", in *Technical Digest, 1986 International Electron Devices Meeting, IEDM '86,* pp. 184-187 (1986).

[6] W. P. Eaton and J. H. Smith, "A CMOS-compatible surface-micromachined pressure sensor for aqueous ultrasonic application", in *Proceedings of Smart Structures and Materials 1995*, SPIE Vol 2448, pp. 258-265(March 1995).

[7] R. D. Nasby, D. L. Hetherington, J. J. Sniegowksi, C. A. Apblett, J. H. Smith, C. C. Barron, W. P. Eaton, and P. J. McWhorter, "Application of chemical mechanical polishing to planarization of surface-micromachined devices", in *Technical Digest: 1996 Solid State Sensor and Actuators Workshop, Hilton Head '96,* pp. 48-53 (June 1996).

[8] T. Lisec, M. Kreutzer, B. Wenk, and B. Wagner, "A combined TMAH and HF sacrificial layer etching technique for surface micromachined devices," in *Proceedings of Micromachining and Microfabrication Process Technology,* SPIE Vol 2639, pp. 286-293(October 1995).

[9] C. H. Mastrangelo, X. Zhang, and W. C. Tang, "Surface micromachined capacitive differential pressure sensor with lithographically-defined silicon diaphragm," in *Digest of Technical Papers: The 8th International Conference on Solid-State Sensors and Actuators, Transducers '95,* pp. 612-619(1995).

[10] SSI Technologies, Inc., 24114 Research Drive, Farmington Hills, MI 48335.

[11] C. H. Mastrangelo and W. C. Tang, "Semiconductor sensor technologies" in *Semiconductor Sensors*, S. M. Sze, Ed., pp. 17-84(1994).

[12] K.E. Bean, "Anisotropic Etching of Silicon", *IEEE Transactions on Electron Devices,* **ED-25**(10), pp. 1185-1193 (Oct. 78).

[13] S. Timoshenko and S. Woinosky-Krieger, *Theory of Plates and Shells*, McGraw Hill Classic Textbook Reissue, (1987).

[14] Motorola, Inc., "Motorola Pressure Sensors," *Sensor Device Data/Handbook,* p. 4.5 (1997).

[15] K.H.-L. Chau, C. D. Fung, P. R. Harris, and J. D. Panagou, "Over-range behavior of sealed-cavity polysilicon pressure sensors," *Sensors and Actuators A*, **28**, pp. 147-152(1991).

[16] P.J. French and A.G.R. Evans, "Piezoresistance in Polysilicon and its Applications to Strain Gauges", *Solid-State Electronics*, **32** (1), pp. 1-10 (1989).

[17] W. P. Eaton and J. H. Smith, "Planar Surface-Micromachined Pressure Sensor with a Sub-Surface Reference Pressure Cavity", in *Proceedings of Micromachined Devices and Components II*, SPIE Vol 2882, pp. 259-265(October 1996).

[18] W. P. Eaton, *Surface Micromachined Pressure Sensors*, Ph.D. Dissertation, The University of New Mexico(May 1997).

Bulk-micromachined sensor   **Surface-micromachined sensor**
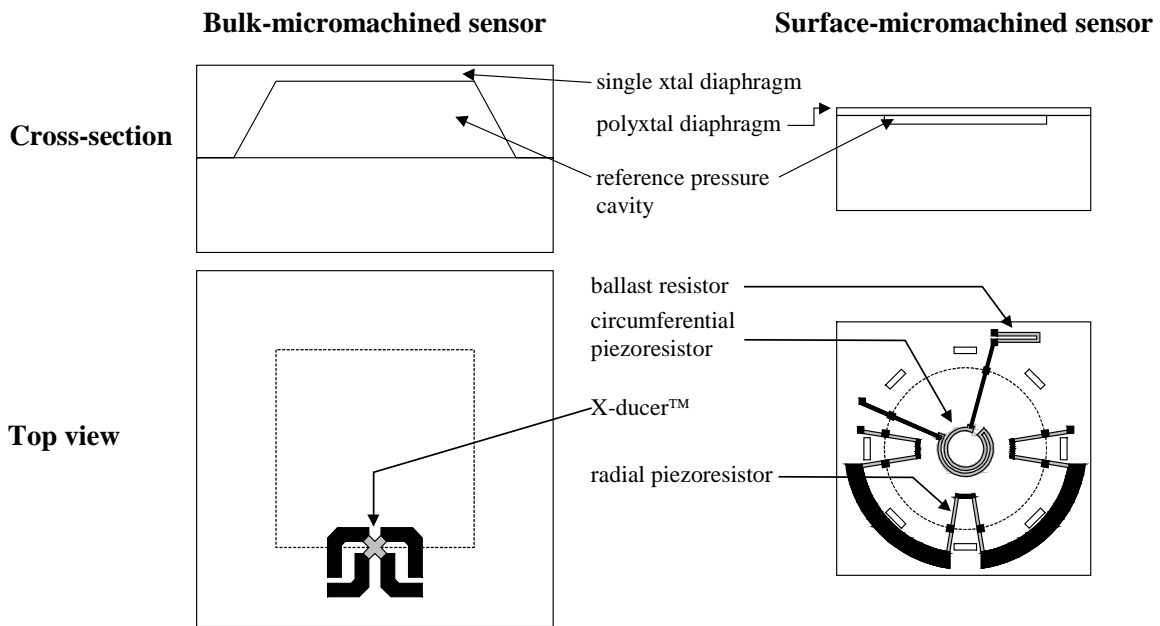

Figure 1. Schematic cross-sections and top view of Motorola bulk micromachined sensor(left) and Sandia surface-micromachined sensor(right). Not to scale.
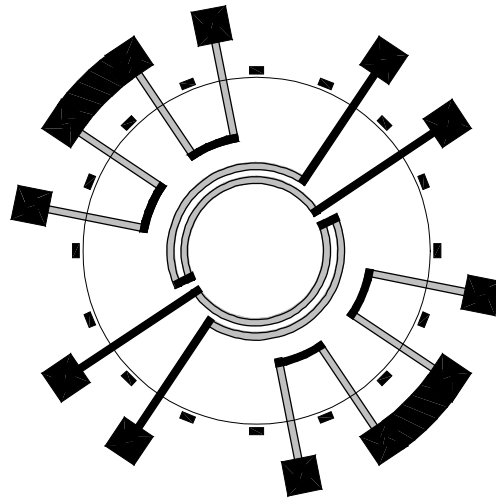

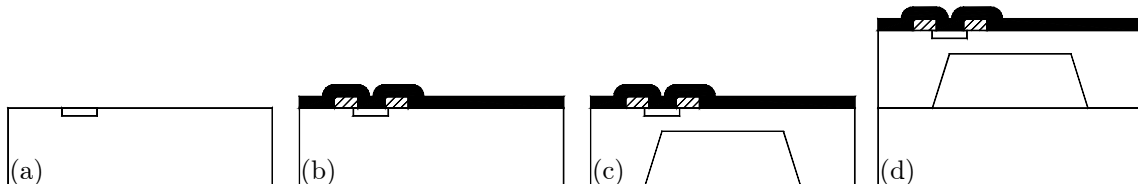**Figure 2. Reference design for single diaphragm Wheatstone bridge sensor.**

Figure 3. Fabrication sequence for BM sensor. (a) ion implant X-ducer™. (b) deposit and pattern metal contacts. passivate with silicon nitride. (c) etch backside of wafer to form diaphragm. (d) bond handle wafer to sensor wafer to form reference cavity.
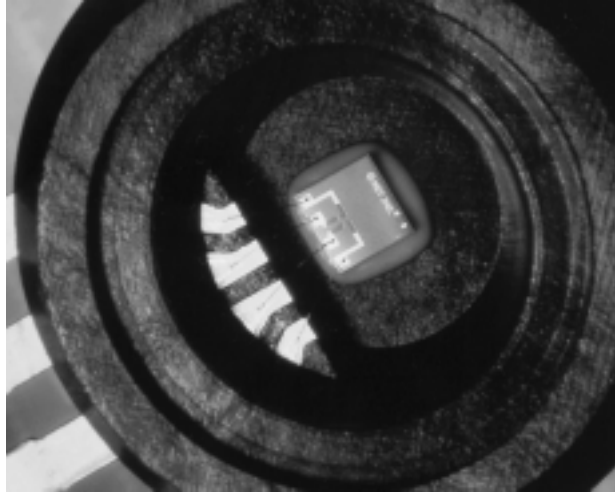
Figure 4. Photograph of MPX200 chip in package without lid.
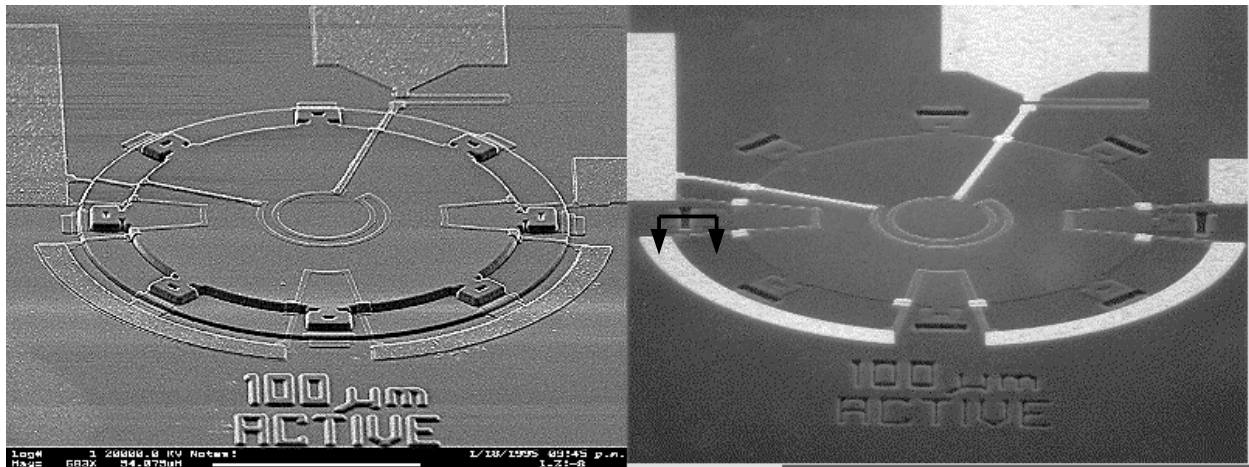
Figure 5. Scanning electron micrographs of 100 µm diameter non-planar(left) and planar(right) SM pressure sensors. Arrows on planar sensor denote the cross section shown in Figure 7.
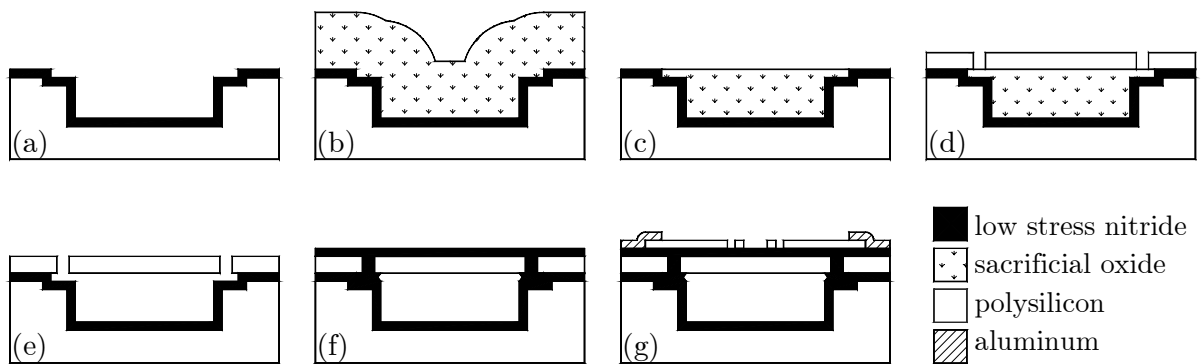

Figure 6. Fabrication sequence for SM sensor. (a) RIE etch deep and shallow trenches. (b) refill trenches with sacrificial oxide. (c) planarize oxide by chemical-mechanical polishing. (d) deposit and pattern diaphragm material. (e) release etch sacrificial oxide in aqueous HF. (f) seal diaphragm with low stress nitride deposition. (g) deposit and pattern polysilicon piezoresistors. deposit and pattern Al metallization.
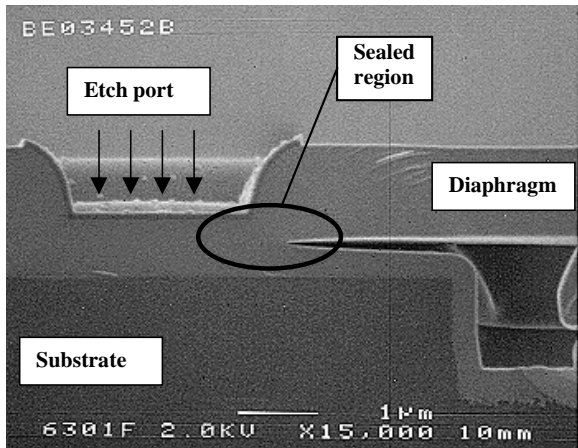
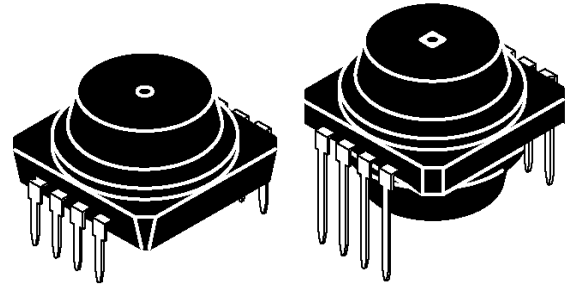**Figure 7. Scanning electron micrograph of sealed etch port.**

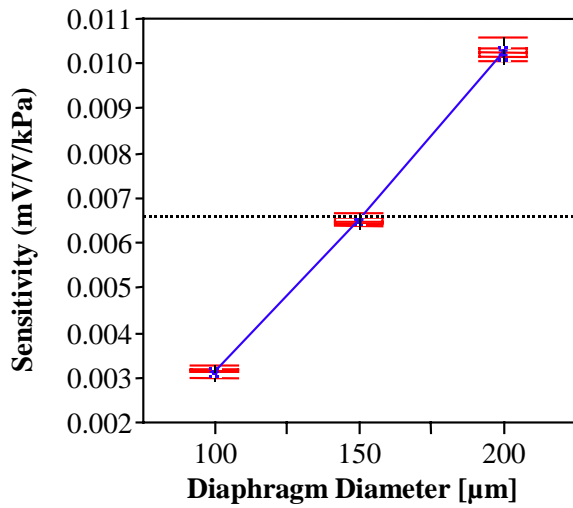**Figure 8. Top(left) and dual(right) piston fit packages.**

Figure 9. SM sensor sensitivity as function of diaphragm diameter.
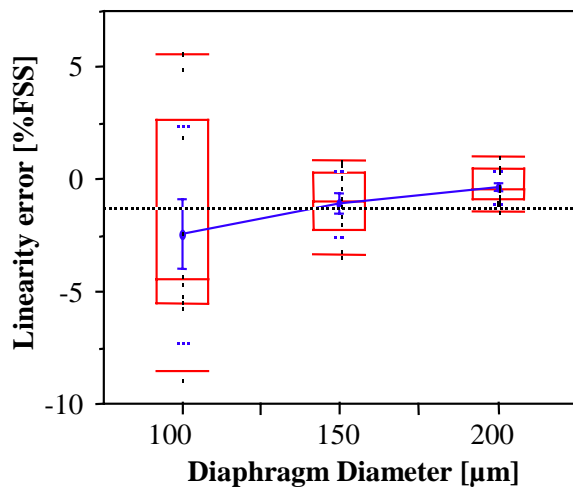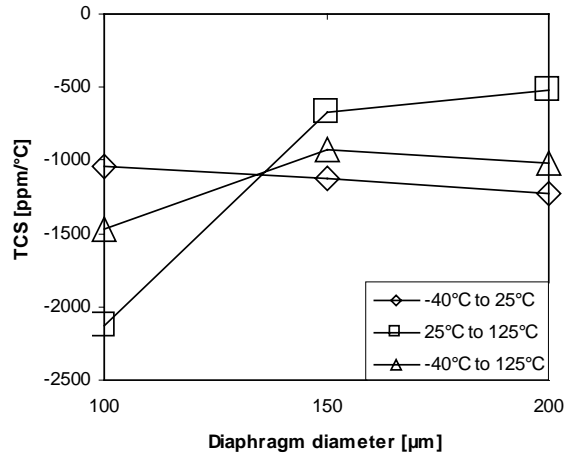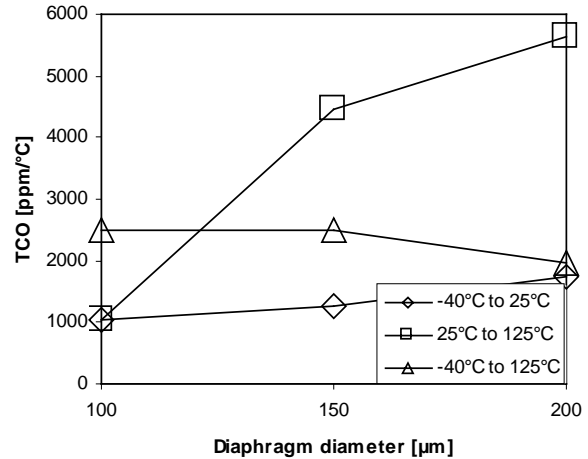

Figure 10. SM sensor linearity error (in percent full scale span) as a function of diaphragm diameter.

Figure 11. Temperature coefficient of sensitivity (TCS) as a function of SM diaphragm diameter calculated over several temperature ranges.

Figure 12. Temperature coefficient of offset(TCO) as a function of diaprhagm diameter calculated over several temperature ranges.

Table 3. 'Data sheet' comparison between MPX200 and SNL pressure sensor.

Parameter	MPX200			Sandia – 200 μm			Units
	Min.	Typical	Max.	Min.	Typical	Max.	
Full Scale Span		20			2		[mV/V]
Offset		7			–27		[mV/V]
Sensitivity		0.1			0.01		[mV/V·kPa]
Linearity Error (± range)	–0.25		0.25	–0.8		0.8	%FSS
Temp. Hysteresis (± range)		0.5			0.8		±%FSS
TCS	–13200		–9600	–907		–549	[ppm/°C]
TCO		750			1950		[ppm/°C]
Input Impedance	400		550	150k		314k	[Ω]
Output Impedance	750		1800	512k		1.1M	[Ω]

Table 4. A/D resolution for two pressure sensors with two different transfer gains with and without 1.6 kHz lowpass filter.

Pressure Sensor	$K_T = 69$			$K_T = 94$		
	Full Scale Span (V)	No Filter (bits)	1.6 kHz Filter (bits)	Full Scale Span (V)	No Filter (bits)	1.6 kHz Filter (bits)
SNL	0.54	3-4	7-8	0.73	3-4	7
MPX200	5.00	9-10	13-14	6.81	9	13